Article:
Li, H, Eshiet, KI-I, Sheng, Y et al. (2018) A parallel-bonded chemical corrosion model for discrete element modelling of chemically corroded limestone. Engineering Fracture Mechanics, 202. pp. 297-310. ISSN: 0013-7944

https://doi.org/10.1016/j.engfracmech.2018.09.028

A parallel-bonded chemical corrosion model for discrete element modelling of chemically corroded limestone

Hao Li [a,b,c], Kenneth Imo-Imo Eshiet [d], Yong Sheng [e], Zuliang Zhong[b,c], Xinrong Liu[b,c], Dongmin Yang[a,*]

[a] School of Civil Engineering, University of Leeds, Leeds, LS2 9JT, UK

[b] School of Civil Engineering, University of Chongqing, Chongqing, 400044, China

[c] National joint engineering research center for prevention and control of environmental geological hazards in the TGR area, Chongqing University, Chongqing, 400045, China

[d] Sustainable Energy Environmental and Educational Development (SEEED) Ltd, Sugarland Texas, TX 77478, USA

[e] Faculty of Science and Engineering, University of Wolverhampton, Wolverhampton, WV1 1LY, UK

Abstract

The mechanical behaviours of rock mass are influenced by the presence of cracks at the microscopic and macroscopic levels. When coupled with corrosion by chemical ions in ground water, these cracks can cause instabilities and fragmentation near the excavated surface of underground structures, such as shield tunnels, *etc*. This paper presents the development of a parallel-bonded chemical corrosion (PCC) model for modelling corroded rocks (limestone). The model extends the bonded-particle model (BPM) by adding a chemically induced damage law to the particle bond. The damage law of the PCC model is derived from Nuclear Magnetic Resonance (NMR) and triaxial compression tests. The PCC model is validated with experimental results and is capable of simulating the micro-damage evolution process as well as predicting the macro-mechanical degradation caused by the chemical corrosion. It is then applied to investigate chemical effects on crack initiation, propagation, coalescence, and the mechanical properties of the limestone containing pre-existing flaws. Microscale correlations are derived linking the crack propagation process, flaw distribution and the effects of chemical corrosion.

Keywords: Distinct element method (DEM); Chemical effects; Nuclear Magnetic Resonance (NMR); Pre-existing flaw; Crack propagation

[*] Corresponding author. Email address: D.Yang@leeds.ac.uk

1 Introduction

Deep subsurface rock mass is often surrounded by water, which contains complex chemical ions that may have different pH values. At the macroscopic level, chemical damage causes various extents of reduction in mechanical properties [1]. At the microscopic level, rock can be viewed as an assemblage of mineral grains, which are often anisotropic in both modulus and strength [2]. In sedimentary rocks, such as limestone and sandstone, the grains adhere to one another by cementitious materials which can deform, break, or be dissolved by chemical solutions [3]. Rock corrosion caused by water accelerates the failure process, leading to mechanical degradation and geological disasters such as landslides and earthquakes [4].

The mechanical behaviour of rock is also influenced by the presence of discontinuities. Such discontinuities are found at all scales, from grain boundaries to joints and regional faults [5, 6]. The existence of discontinuities, such as joints, cracks, *etc.,* in rock mass has two main effects: (1) by reducing the intact section inside rock, these discontinuities decrease the strength of the rock; (2) under external stress, new discontinuities may initiate from the existing cracks, and propagate and connect with other cracks, further decreasing the strength of the rock [7, 8]. Coupled with chemical effects, the mechanical behavior, and the crack propagation and connection processes may be more complicated. Therefore, it is important to investigate the micro damage caused by chemical effects and the process of crack initiation, propagation, coalescence as well as the failure mechanisms of rock under coupled chemical-mechanical impacts during their use for rock engineering applications, such as tunnels, foundations and slopes, and hydrocarbon and geothermal energy extraction [9].

Over the past few years, considerable laboratory tests have been carried out to investigate the macroscopic and microscopic mechanical properties of rock without pre-existing cracks and under various chemical environments [10-13, 5, 14-16]. However, it is still very difficult for real-time monitoring of laboratory experiments designed to quantitatively analyse the chemical corrosion process of rock while subjected to loading. To have a better understanding of crack initiation, propagation and coalescence processes during external rock compression, indirect techniques, such as acoustic emission (AE) [17-19], computerised tomography (CT) scan [20-22], microscopic observation (petrographical thin section, SEM/ESEM) and high-speed camera are sometimes used [23].

In physical lab tests, the detection of crack propagation of rock samples with pre-existing flaws, especially for crack initiation, is based on the first distinct cracking sound or the first

minute crack opening observed on the specimen surface. However, as shown in other experimental studies employing AE [24] and CT [25] techniques, cracking events prior to those observed on the surface may occur inside the rock specimens. Even when shear failure bands can be distinguished, the AE and CT resolution is often too low to capture the development of distinct crack trajectories [26, 27].

Numerical modelling of rock mechanics and rock engineering processes enables easier and detailed investigation and visualization of micro cracks, stress distributions and other variables [28-32]. Using extended finite element method (XFEM), Mohtarami *et al*., [33] conducted three-point and four-point bending tests on chemically corroded rock samples to investigate the crack propagation law. The results show that the deformability of the sample increase with the growth of the chemical ions concentration; fracture toughness of the sample decrease with the growth of pH values of the solutions. Abdelghani *et al*., [34] used Hydro-Geosphere, a numerical tool, to analyze unsaturated water flow in an open pit filled with mining wastes. This involved water flow and solute transport effects associated with recharge, waste material and fractures of the in the surround rock mass.

Discrete Element Method (DEM) is a rapidly developing area in computational mechanics. This modelling approach which represents rock as an assemblage of particles (spheres, ellipsoids, blocks) that interact with each other, has been recognised as both a scientific tool and an engineering tool to investigate the mechanic properties of rock in both microscopic and macroscopic scales [35]. Bonded particle model (BPM), based on DEM, constitutes a dense packing of non-uniform sized circular or spherical particles [36]. All particles are bonded together by bonds that have specific stiffness and strength. These particles can be detached when external loads exceed the bond strength [37].

BPM is widely used for modelling the mechanical behavior of rock. Asadi *et al.,* [38] conducted direct shear tests by using BPM to simulate the fracture of synthetic rocks and to investigate the effect of micro-properties shear fracture. Different kinds of failure including asperity sliding, cut-off, and asperity degradation were explicitly observed and evaluated. Zhang *et al.* [39] used BPM to investigate pore size and distribution effects on the uniaxial compressive strength (UCS) of lithophysal rocks. Their results show that UCS decreases when pore radii increase but decreases due to the existence of pores with the same condition of porosity. Most previous studies focus on mechanical properties such as elastic and plastic deformations, and failure mechanisms of intact rocks [40, 41], or the relationship between

modelling parameters and mechanical properties of intact rocks [42]. Research on the micro damage investigation and the crack propagation of chemically corroded rock using BPM in DEM is rare.

This paper presents a parallel-bonded chemical corrosion (PCC) model, which extends the features of the bonded-particle model (BPM) by adding a damage evolution law to the parallel bond. Limestone is used as an example rock type. Before mimicking the chemical corrosion processes using the PCC model in DEM, laboratory chemical corrosion tests on limestone are first conducted to investigate the micro damage evolution using Nuclear Magnetic Resonance (NMR). Internal microstructure images and T_2 values (transverse relaxation time distribution, which depends on the size of water-saturated pores) for chemically corroded limestone are obtained. Based on the experimental data, a micro damage cumulative model of the corroded limestone is proposed and then implemented in the BPM (with parallel bond) to form the PCC model. The PCC model is applied for DEM simulations to investigate chemical effects on crack initiation, propagation, coalescence, and the mechanical properties of the limestone containing pre-existing flaws. Microscale correlations are derived linking the crack propagation process, flaw distribution and the effects of chemical corrosion.

2 Micro damage evolution in chemical corroded limestone

2.1 Experimental methods

Microscopic damage is the root cause of macroscopic mechanical degradation. To quantify damage at the microscale and construct the micro damage model of the rock during chemical corrosion, a damage variable must be defined. In this paper porosity is selected as the key parameter of the damage variable D, calculated as [44]:

$$D = \frac{V - V_D}{V} = \frac{n - n_0}{1 - n_0} \quad (1)$$

Where, D is the damage variable, V is the volume of the sample, VD is the volume of the damaged part of the sample, n_0 is the porosity of the sample in air, and n is the porosity of the sample after being subjected to external damage, such as chemical corrosion or loads.

In this paper, building upon our previous work [43], the initial porosity and the porosity after chemical corrosion are both measured by NMR, which is shown in Fig.1 (a). The NMR system measures the signal intensity of hydrogen atoms, which depends on the number and size of pores inside a fully-saturated rock. The NMR machine mainly detects the NMR signal

of the hydrogen nucleus (1H) from fluids, such as water, within the rock pores and outputs transverse relaxation time distribution (T2 spectrum), porosity and Magnetic Resonance Imaging (MRI), which can be used to investigate the pore size distribution and micro structure damage of the rock. Thus, when rock sample is fully saturated with water, the NMR system can analyze the detected the pore volume and the pore size distribution. The test cell of the rock testing system, as is shown in Fig.1 (b), is used to conduct mechanical compression tests.

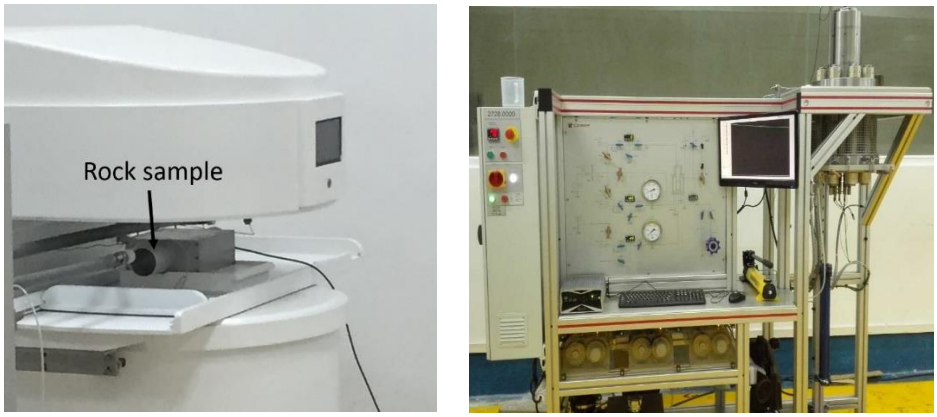

(a) (b)

Fig.1 NMR system and test cell of rock testing system

Limestone is chosen as the test sample in this study. The limestone blocks, which are selected from a single block without macroscopic cracks, are machined into cylindrical shapes with a length of 100 mm and a diameter of 50 mm. From X-ray diffraction (XRD) analyses it is found that the limestone samples are composed of 95% calcspar, quartz, cements and 5% other minerals. According to water sample analysis, which is collected near the rock collection site, the pH value of the water sample is 6.5 and the main ions are Na^+, Ca^{2+}, Mg^{2+}, SO_4^{2-}, Cl^- and HCO^-. To simplify the experimental study, the complex ionic composition of the water is replaced by Na_2SO_4 solution, which is made by NaCl solution added with H_2SO_4. Three Na_2SO_4 solutions with pH values 3, 5, 7, as well as distilled water, are used. All the initial concentrations of the solutions are 0.01 $mol \cdot L^{-1}$. The procedure of the tests is as follows:

The samples are saturated using a vacuum saturation device. After saturation for 24h, initial porosities of samples are measured using NMR and those with similar values are categorized into four groups. Then, these samples are immersed in distilled water and Na_2SO_4 solutions

with three pH values (3, 5 and 7) for three designed periods (20d, 40d and 60d), as listed in Table 1.

Table 1 Group of samples

No. of specimen	pH	Time/d	No. of specimen	pH	Time/d
A-1	3	20	C-1	3	60
A-2	5	20	C -2	5	60
A-3	7	20	C -3	7	60
B-1	3	40	D-1	Distilled Water	20
B -2	5	40	D-2	Distilled Water	40
B -3	7	40	D-3	Distilled Water	60

When the samples reach the designed erosion period, NMR tests are conducted to analyse the porosity change. After the NMR tests, the samples are taken out of the NMR machine and put in the triaxial pressure cell of the rock test system for triaxial compression tests. The confining pressure is gradually increased up to 10 MPa and then fixed. After that, a strain control mode is used for the axial loading at a rate of 0.02 $mm \cdot min^{-1}$ until the sample is ruptured.

2.2 Test results

Porosity changes obtained by NMR are listed in Table 2. The damage evolution rate is calculated according to Equation 1, and the relationship between damage evolution and corrosion time is shown in Fig.2.

Table 2 Porosity change of limestone samples after chemical corrosion

NO of samples	Time/d	pH	Initial Porosity	Corrosion Porosity	Porosity Change/%
A-1	20	3	5.43	6.68	23.2
A-2	20	5	5.37	5.85	9.2
A-3	20	7	5.38	5.62	4.4
B-1	40	3	5.35	7.02	31.2
B-2	40	5	5.31	6.03	13.6
B-3	40	7	5.36	5.72	6.8
C-1	60	3	5.46	7.62	39.6

C-2	60	5	5.36	6.71	25.2
C-3	60	7	5.32	5.85	9.1
D-1	20	Distilled Water	5.39	5.44	1.1
D-2	40	Distilled Water	5.34	5.49	2.8
D-3	60	Distilled Water	5.33	5.54	4.1

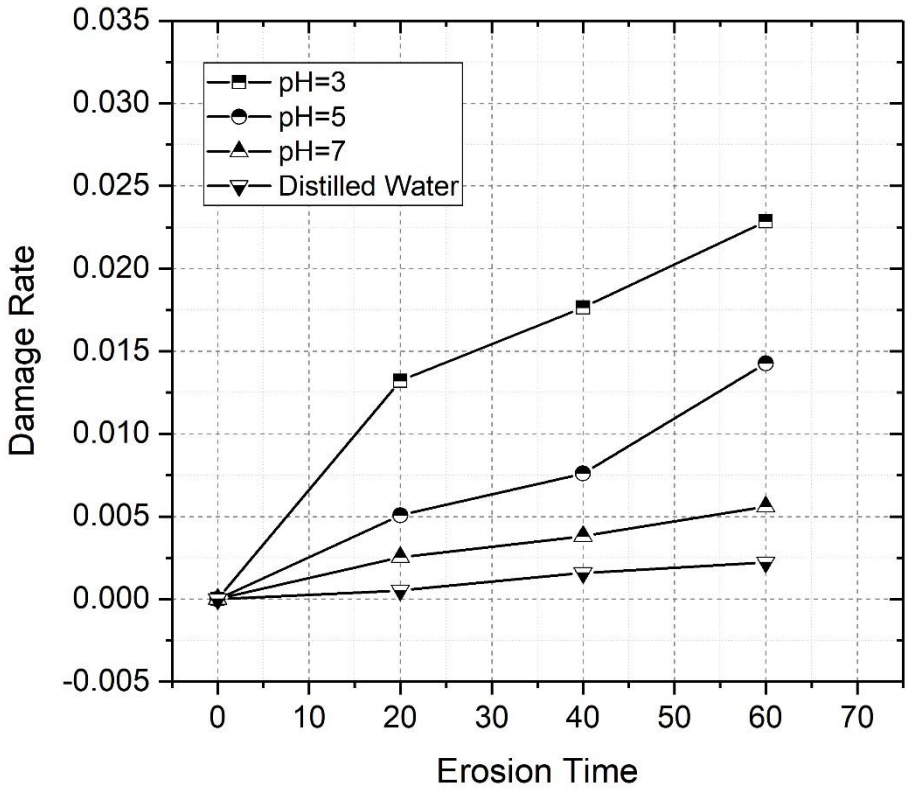

Fig.2 Damage rate of limestone after different chemical corrosion time

It can be seen from the Fig.2 and Table 2 that the porosities of the original samples are relatively low, having an average value of about 5.4%. However, chemical corrosion caused an increased in micro damage of the limestone samples with immersion days. The damage on limestone samples immersed in the most acidic solution (pH value of 3) is significantly higher with a faster growth rate in comparison with other solutions for the same period of time. As expected, samples softened by distilled water have the least damage.

Fitted by Fig.2, the relationship between micro damage and chemical corrosion can be expressed as follows:

$$D_r = \alpha_1 t^2 + \alpha_2 t + c \qquad (2)$$

Where, D_r is the micro damage caused by chemical corrosion, $\alpha_1$and α_2 are the parameters related with the pH value and the chemical ions of the solution, and c is a constant, which can be fitted by test data. It is noted that micro damage is a quadratic function of chemical corrosion time. This function will be used as a base formula for the degradation of parallel bond in the PCC model described in next section.

3 PCC Model formulation and implementation

3.1 Bonded particle model (BPM) with parallel bond

In the BPM the parallel bond which connects two particles resists both forces and moments applied to the particles, as shown in Fig.3. The following five parameters define a parallel bond: λ, radius multiplier defined such that the parallel-bond radius equals this multiplier times the minimum radius of the two bonded balls; k_n , parallel-bond normal stiffness; k_s, parallel bond shear stiffness; σ_c , parallel bond normal strength; τ_c , parallel bond shear strength. Details of the parallel bond have been described in [36] and only the forces and moments calculations are briefly introduced here.

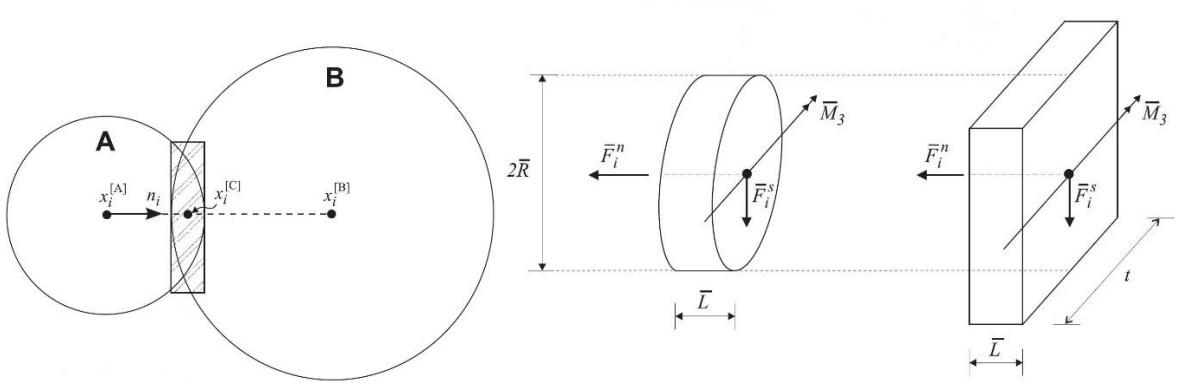

(a) (b)

Fig.3 Parallel bond depicted as a finite sized material [36]

The total force and moment associated with the parallel bond are denoted by F_i and M_3, which are shown in Fig 3. And the force vector can be resolved into normal and shear components with respect to the contact plane as:

$$F_i = F_i^n + F_i^s \qquad (3)$$

Where F_i^n and F_i^s denote the normal and shear force component vectors, respectively. The force and moment vectors are shown in Figure 3, where the parallel bond is depicted as a finite-sized piece of elastic material.

When the bond is formed F_i and M_3 are initialized to zero. Each subsequent relative displacement and rotation-increment at the contact results in an increment of elastic force and moment that is added to the current values. The elastic force-increment and the elastic moment-increment occurring over a time step of Δt are calculated by [36]:

$$\begin{cases} \Delta F_i^n = k^n A U^n \\ \Delta F_i^s = k^s A U^s \\ \Delta M_3 = -k^n I \Delta\theta^3 \end{cases} \quad (4)$$

Where ΔF_i^n, ΔF_i^s and ΔM_3 are axial and shear directed forces and moment, respectively; U^n, U^s and $\Delta\theta^3$ are the axial and shear directed relative displacements and rotation between the two bonded particles; A is the area of the bond cross-section, and I is the moment of inertia of the bond cross-section about an axis through the contact point and in the direction of $\Delta\theta^3$, which are calculated by [36]:

$$\begin{cases} A = 2Rt \\ I = \frac{2}{3}R^3 t \end{cases} \quad (5)$$

The maximum tensile and shear stresses acting on the bond periphery are calculated to be:

$$\begin{cases} \sigma_{max} = \frac{-F^n}{A} + \frac{|M_3|}{I} R \\ \tau_{max} = \frac{F_i^s}{A} \end{cases} \quad (6)$$

If the maximum tensile stress equals/exceeds the normal strength ($\sigma_{max} \geq \sigma_c$), or if the maximum shear stress equals/exceeds the shear strength ($\tau_{max} \geq \tau_c$), then the parallel bond breaks.

3.2 Damage evolution due to chemical effects

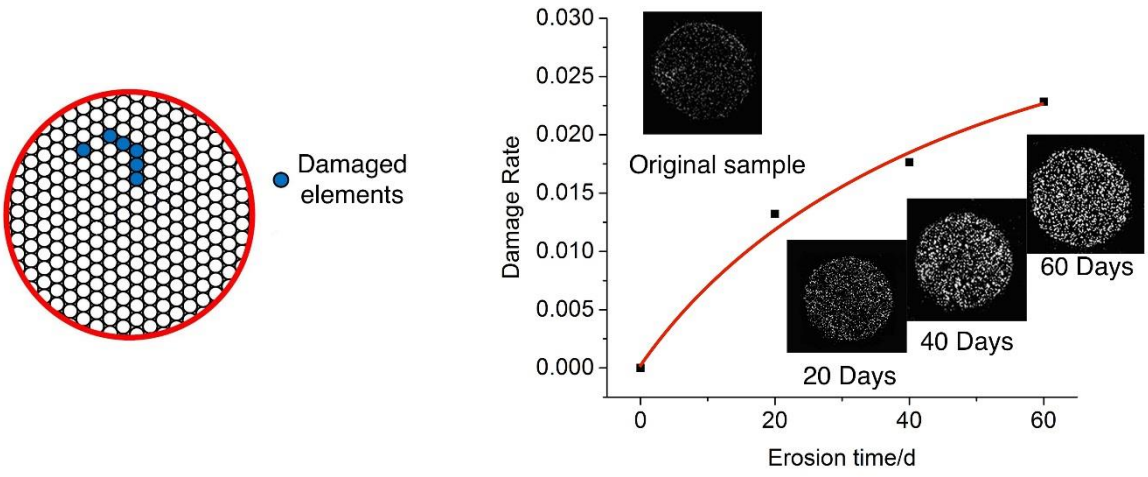

(a) (b)

Fig. 4 MRI of micro damage evolution with increased chemical immersion period

Grains in limestone are glued together by some kind of cement, for instance quartz, calcite, or clay minerals. The macro mechanical properties of limestone rely on the strength of the cementing material [45]. Factors that contribute to the micro damage development and mechanical properties degradation mainly include dissolution and chemical reaction. Water acts as a solvent, thus some mineral particles in the rock in contact with water will dissolve and become diffused in the aqueous solution to a certain degree. This leads to an increase in porosity and softening of rock structure. At the same time, there are chemical reactions, since some minerals in rock react easily with chemical ions in the solution; this process can form new minerals and change the micro structure of the rock [46], as shown in Fig.4 (a).

The Magnetic Resonance Imaging (MRI) of the inner section of limestone immersed in pH3 solution and its micro damage evolution curve are shown in Fig.4 (b) as an example. The white points in the images reflect the water inside the rock and the black area is the background. The brightness and the number of white points of the image increase when the porosity increases. It can be seen that: (1) after chemical corrosion, there is a significant increase of white points and brightness, which indicates the calcspar inside the limestone is been dissolved so that the porosity and the micro damage of the sample increases; (2) As expected, the damage evolution curve is convex, indicating the damage growth rate decreases with the immersion time. According to chemical reaction rate theory [46], after a period of chemical reaction, the concentration of the chemical ions, such as H^+ ions, in the chemical

solution decreases, thus the reaction rate between chemical ions and materials in rock decreases.

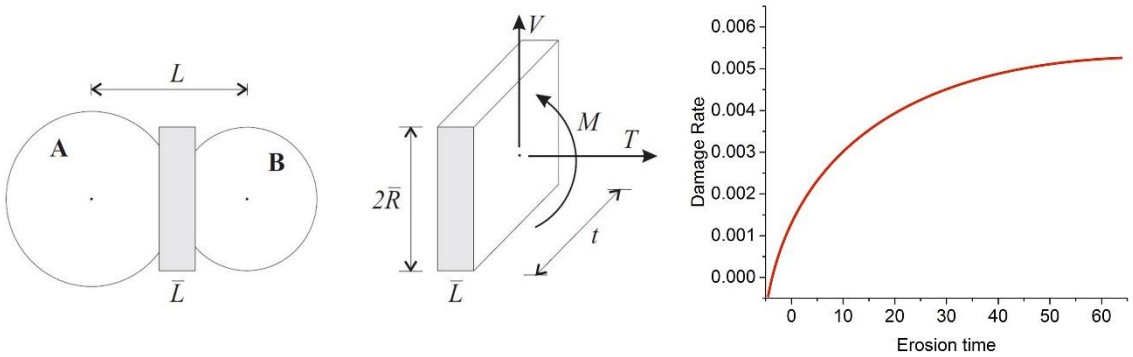

(a) (b)

Fig.5 BPM and bond damage law for PCC model

Compared with the corrosion mechanism of rock, BPM in DEM represents rock at the grain scale by a dense packing of non-uniform-sized circular or spherical particles that are bonded together at their contact points as shown in Fig.5 (a). Damage is represented explicitly as broken bonds (which will be referred to as micro cracks) that may form when load is applied [47]. Thus, the chemical corrosion process can be implemented by reducing or removing the bonding material between the particles at a specified rate that is based on the damage evolution law developed from the NMR tests. The micro damage equation of rock corroded by chemical solutions is presented in Equation 2. However, it cannot be directly adopted to the PCC model, because the particle size of the DEM model is larger than those in real rocks [48]. According to the relationship chemical reaction rate theory and the test data in this study [46], the relationship curve of chemical damage and corrosion time is convex. To simulate the chemical effects in DEM, the relationship curve for bond damage rate and chemical corrosion time should also be convex and similar to the micro damage curve obtained by the laboratory results in Section 2, which is shown in Fig.5 (b). Thus, the equation of the damage evolution equation in the PCC model has a form similar to Equation 2, but the three constants could be different and fitted by inverse analysis from laboratory test data.

3.3 Acquisition of damage law for PCC model

3.3.1 Calibration of BPM model for limestone in air

This study is mainly based on the two-dimensional particle flow code (PFC2D), which is based on the principles of DEM. In general, DEM simulations show good qualitative

agreement with experimental observations [49]. However, the mechanical properties of a DEM model are usually specified at the micro-scale, *e.g*. particle stiffness, parallel bond strengths and the friction coefficient between particles [35]. This is different from the real rock, which is usually described by their elastic modulus, peak strength, Poisson's ratio, tensile strength, etc. Thus, the use of this approach for real problems requires a calibration process [29]. With NMR tests as well as triaxial compression tests, the properties of particles and parallel bonds in BPM can be calibrated. The minimum radius of particles of the DEM sample is $1.5e^{-2}$ mm, and the maximum-to-minimum radius ratio of the particles is 1.66. The parameters used in PFC2D for limestone sample in air are listed in Table 3. The mechanical properties obtained from laboratory test and PFC simulations are shown in Table 4, confirming that the calibrated DEM model can accurately represent the mechanical behaviour of limestone sample in air.

Table 3 Parameters in PFC2D for limestone sample in air

Ball density[kg/m3]	2650	Ball stiffness ratio	1
Ball-ball contact modulus [Pa]	3.5×10^{10}	Parallel-bond normal strength, mean [Pa]	1.85×10^{8}
Parallel-bond radius multiplier	1	Parallel-bond shear strength, mean [Pa]	1.85×10^{8}
Parallel-bond modulus [Pa]	3.5×10^{10}	Parallel-bond normal strength, std. dev. [Pa]	4.5×10^{7}
Ball friction coefficient	0.5	Parallel-bond shear strength, std. dev. [Pa]	4.5×10^{7}

Table 4 Main macro mechanical properties of limestone obtained from lab tests and DEM simulations

Mechanical property	Experiment tests	DEM simulations
Peak strength (MPa)	230.32	238.47
Elastic modulus *E* (GPa)	55.45	56.60
Poisson's ratio *v*	0.23	0.24

3.3.2 Bond damage in PCC model for chemical corroded limestone

The PCC model idealizes the sedimentary rock as a cemented granular material and then reduces the diameter of the cement bond based on the micro damage cumulative model. It is followed by these assumptions:

(1) The chemical reaction only affects the cement; it does not affect the grains. Therefore, each parallel bond is a potential reaction site.

(2) The reaction occurs at the bond surface and removes the bond material at a uniform rate which can be called the corrosion rate. The corrosion rate depends on the pH value and the ions of the chemical solution.

The reduction in parallel-bond diameter during the chemical corrosion process is specified by the bond damage ratio D_p, which is shown in Fig.5 (b) and is expressed as:

$$D_p = \frac{R-R_c}{R} = \frac{\lambda-\lambda_c}{\lambda} \qquad (7)$$

Where R_c is the parallel bond diameter after chemical corrosion, R is the intact parallel bond diameter, λ_c is the bond radius multiplier after chemical corrosion, λ is the intact bond radius multiplier. Thus, R_c can be expressed as:

$$R_c = (1 - D_p)R \qquad (8)$$

Inverse analysis is carried out to obtain the damage evolution law for the bond degradation rate D_p in the PCC model for chemical corroded limestone. The three steps are executed in PFC2D to simulate the chemical corrosion process of corroded limestone.

(1) Reduce the diameters of all parallel bonds according to Eq. (7) and Eq. (8).

(2) Execute biaxial compression tests (confining pressure 10MPa) with the damaged bonds in PFC2D until the sample is completely fractured.

(3) Compare the mechanical properties obtained from PFC2D simulations and the laboratory tests, until DEM model can well represent the mechanical behaviours of chemical corroded limestone samples, particularly the peak strength. If not, return to step 1.

The peak strength of the lab tested samples and the PCC simulated samples are shown in Fig. 6. After biaxial test, the fracture patterns of the corroded sample and crack zones of the

sample simulated by PCC model are compared (Table 5). The PCC model is in good agreement with laboratory tests (Table 5 and Fig.6).

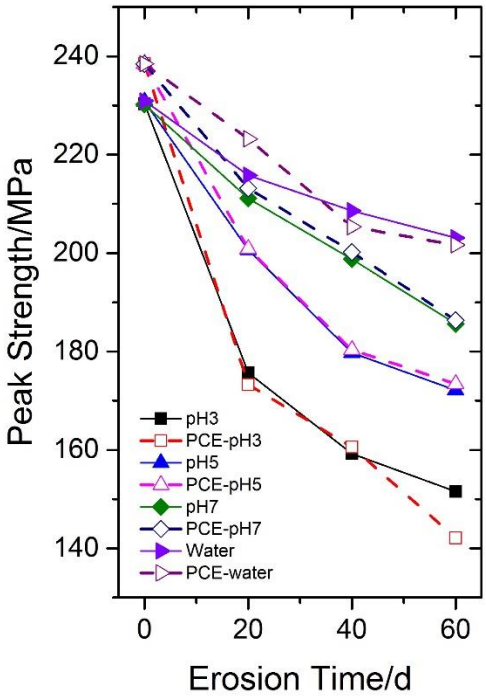

Fig.6 Peak strength of the limestone samples in laboratory tests and from PCC simulations

Table 5 Comparison of fracture patterns from lab tests and DEM simulations

pH value	Fractured sample	Sketch of the fracture pattern	Cracks in DEM simulation
pH3		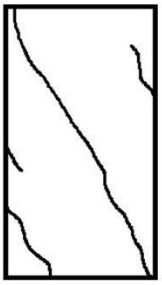	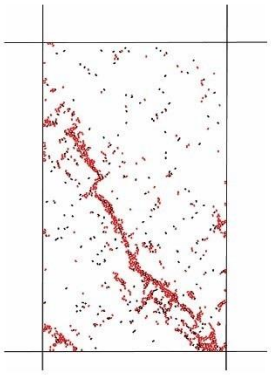
pH5		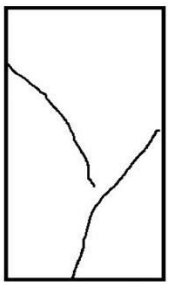	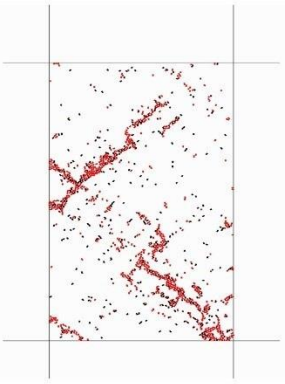
pH7		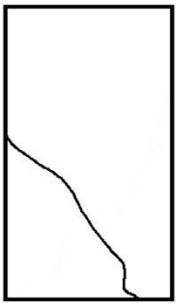	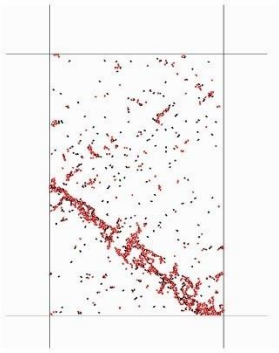
Distilled water		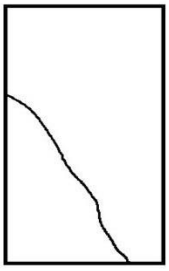	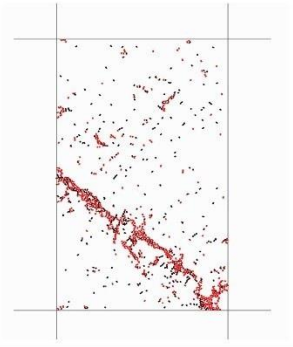

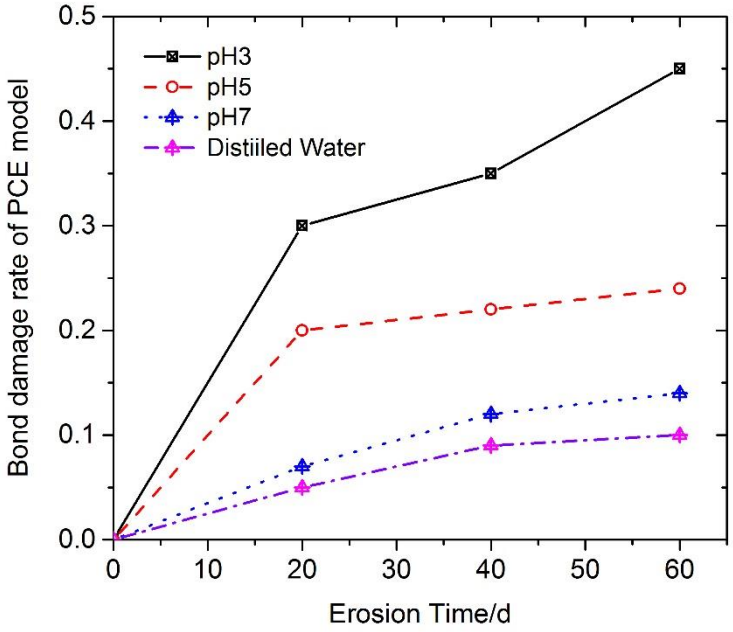

Fig.7 Change of bond degradation rate with chemical corrosion time

The relationship of bond degradation rate and corrosion time is shown in Fig.7. The bond degradation curve of the PCC model is similar to the micro damage curve from NMR tests. The bond damage of the sample corroded by pH3 solution is always more severe and grows faster than other sample, and the bond degradation rate of water softened sample is the lowest. Thus, the corrosion kinetic of PCC model can be expressed as:

$$D_p = \beta_1 t^2 + \beta_2 t + c \qquad (9)$$

Where, D_p is the bond damage caused by chemical corrosion; β_1 and β_2 are material parameters that vary with the chemical environment; and c is the constant. With the damage kinetics D_p, the bond damage evolution law provides the rate at which a parallel bond degrades. The bond becomes weaker as the chemical corrosion proceeds so that the effective bond stiffness decreases, which allows for a macroscopic load redistribution to occur throughout the material.

The constant values are determined by fitting the DEM simulation data in Fig.7, and are shown in Table 6.

Table 6 Parameters of bond degradation formula

Chemical solution	β_1	β_2	c
pH3 Na_2SO_4	-1.25×10^{-4}	0.015	0.015
pH5 Na_2SO_4	-1.12×10^{-4}	0.11	0.009
pH7 Na_2SO_4	-3.12×10^{-5}	0.004	5×10^{-4}
Distilled water	-2.5×10^{-5}	0.003	1.2×10^{-4}

After the diameter of a parallel bond is reduced due to chemical corrosion, both the effective stiffness and the bond force will also be reduced. This is due to the reduction in the bond cross-sectional properties *A* and *I*. The bond cross-sectional properties after chemical corrosion can be expressed as:

$$\begin{cases} A_c = AD_p \\ I_c = ID_p^3 \end{cases} \quad (10)$$

Where A_c and I_c are the bond cross-sectional properties after chemical corrosion. By using Eq. (10), the new parameter can be inserted. Based on NMR and mechanical tests of the chemically corroded limestone samples, the chemically induced damage law is obtained, which is shown in Fig 4. The corrosion kinetics of the PCC model is derived according to the damage process of the chemically corroded limestone samples, expressed by Equation (9) with parameters presented in Table 6. By using the PCC model, the mechanical properties of the limestone corroded by chemical solution for random periods can be predicted.

4 Application of the PCC model: investigating crack propagation and coalescence

In this section, the PCC model will be applied to investigate crack propagation, coalescence and the mechanical properties of the chemically corroded rock with pre-existing cracks. Effects of the pre-existing crack distribution on the mechanical properties of the rock, as well as the crack propagation along the rock bridge between the flaws is also analyzed.

4.1 Model setup for BPM

The modelled limestone samples are cylindrical shaped with a length of 100 mm and a diameter of 50 mm. All the parameters of the numerical sample are shown in Table 3. All the samples are corroded by chemical solution or soften by distilled water for 60 days, which is as same as the test condition mentioned in Section 2, so that the chemical damage caused by

chemical ions are same as that in previous test study. Two flaws of 4 mm each in length are created in per sample, as shown in Fig.8.

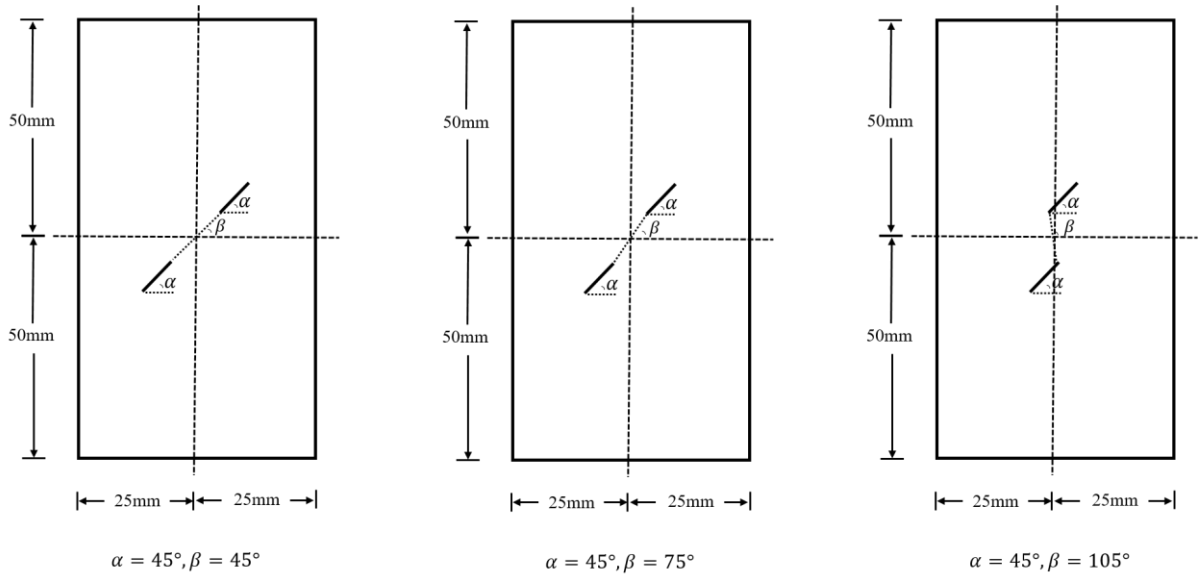

Fig.8 Layout of limestone specimens with two or three flaws

The pH value of the chemical solution are 3, 5 and 7, to investigate of the chemical solution on strength and the crack propagation process in limestone samples. The sample immersed in distilled water is used as a control. The sample groups are listed in Table 7.

Table 7 Group of samples

No. of sample	Chemical solution	Flaw distribution	No. of sample	Chemical solution	Flaw distribution
A-1	In air	α=45°, β=45°	C-3	pH5	α =45°, β =105°
A-2	In air	α =45°, β =75°	D-1	pH7	α=45°, β=45°
A-3	In air	α =45°, β =105°	D-2	pH7	α =45°, β =75°
B-1	pH3	α=45°, β=45°	D-3	pH7	α =45°, β =105°
B-2	pH3	α =45°, β =75°	E-1	Distilled water	α=45°, β=45°
B-3	pH3	α =45°, β =105°	E-2	Distilled water	α =45°, β =75°
C-1	pH5	α=45°, β=45°	E-3	Distilled water	α =45°, β =105°
C-2	pH5	α =45°, β =75°			

After the calibration process with the intact rock sample without pre-existing flaws, two open straight flaw is created by deleting particles in the model center and along the desired flaw direction. A typical numerical sample is shown in Fig.9.

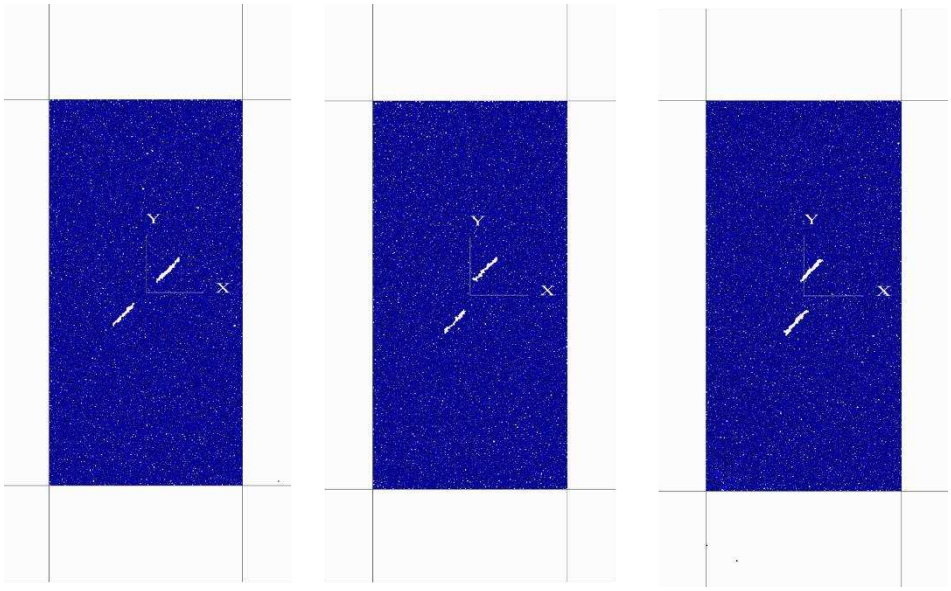

Fig.9 Rock sample in BPM containing two pre-existing flaws

Due to the heterogeneity and randomness introduced in PFC with regard to the micro-strength values, and the arbitrarily generated particle radius, no two runs produce the same results [50]. This feature allows a more realistic numerical simulation of the nature of rock material. In the BPM used in this study, a crack is formed when a parallel bond between adjacent parent particles is broken [36]. In order to have a comprehensive result of the crack propagation in the limestone sample, each flaw inclination with the same set of parameters is repeatedly run five times and a comparison of the results used to generalize the pattern of cracking.

4.2 First cracks of the sample in BPM

The first cracks initiated from pre-existing flaws, in which the tensile crack is red and the shear crack is black are shown in Fig.10. The results in Fig.10 are chosen from the sample in air and that corroded by pH3, due to the similarity of results from other groups.

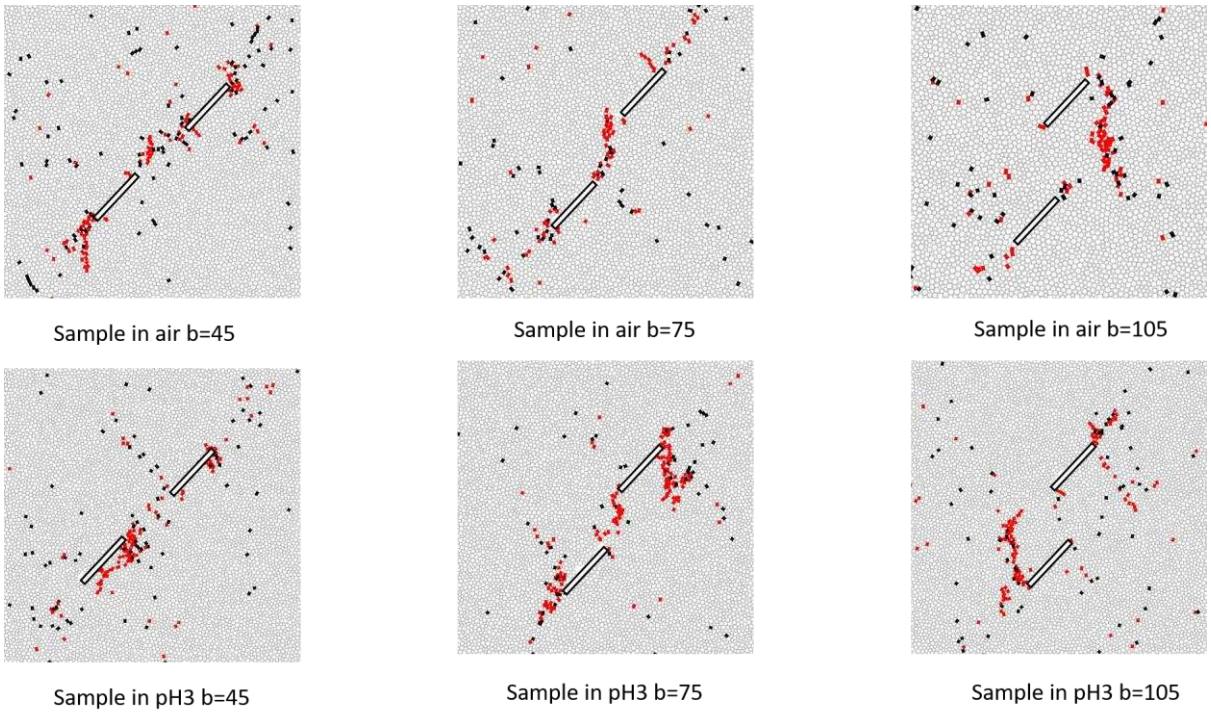

Fig.10 BPM modelling results of the first cracks from pre-existing flaws oriented at different flaw inclination angles.

The following are observed from the test samples: 1) irrespective of the chemically eroded state of the rock, the first set of micro cracks are tensile, which are typically initiated from the pre-existing flaws and propagate in the direction of the vertical stress; 2) tensile wing cracks are the first to be initiated at the bridge region between the two pre-existing flaws. At lower angles of bridge (β) inclination such as 45^o and 75^o, wing cracks are likely to connect to bigger macro cracks with increasing loading, whereas, at higher angles of bridge inclination, such as 105^o, wing cracks are isolated and do not connect with other forms of cracks.

In BPM, the peak stress and the first crack initiation stress, regarded as the stress corresponding to the initiation of the first observable crack in the numerical sample are obtained, as shown in Table 8 and Fig.11, respectively. The first crack initiation stress ratio (n_1) is calculated as follows:

$$n_1 = \frac{\sigma_i}{\sigma_p} \tag{11}$$

Where σ_i is the first crack initiation stress of the sample, which is the average values of the results obtained from five calculation runs; and σ_p is the peak stress of the sample, which is also the average values of the results obtained from five simulations.

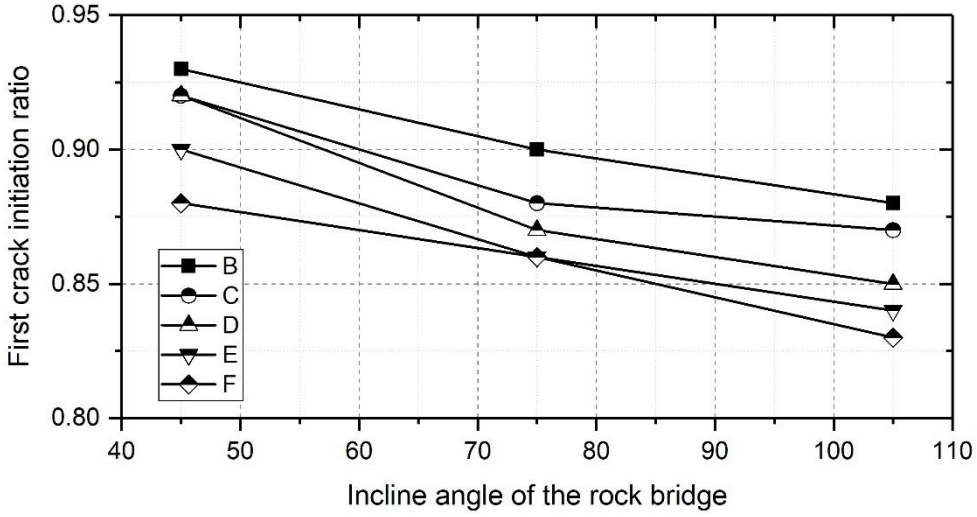

Fig.11First crack initiation ratio vs incline angle of the rock bridge

Table 8 Peak strength of the limestone sample in DEM

Incline angle β (°)	ph3 (MPa)	ph5 (MPa)	ph7 (MPa)	water (MPa)	air (MPa)
45	93	118	138	144	165
75	92	121	143	149	170
105	96	123	145	152	175

It can be observed from Fig.11 and Table 8 that the chemical effects has a significant influence on the peak strength of the limestone samples even when they have different flaw arrangements. Due to the chemical effects, the peak strength of the sample decreased. Samples corroded by the pH3 solution experienced the biggest strength degradation compared with that corroded by other pH values solution. Samples softened by only distilled water have the smallest strength degradation. The first crack initiation ratio of the sample corroded by the pH3 solution is higher than that in other groups; the water solution gives the lowest ratio. This is due to the chemical reaction between the mineral components in limestone sample with the ions in the chemical solution, which weakens the rock strength so that cracks are easier developed. These results are in good agreement with those obtained from the lab tests on limestone samples without flaws [43].

The flaw pattern also influences the first crack initiation stress. Samples with lower bridge inclination angles, such as b=45, have higher first crack initiation stress but lower peak

strength, compared with samples with higher bridge inclination angles. This means that lower rock bridge inclination angles enables easier development and coalescence of micro cracks, such that rock masses of this nature fail more easily under external loads.

4.3 Crack propagation process of the sample in BPM

During the loading process, crack development and propagation process occurs in three stages [51, 52]: crack initiation, secondary crack generation stage and failure. Typical three stages of samples under chemical effects (pH3) and their corresponding stress-strain curve are shown in Fig.12. The pattern of crack propagation and connections is similar for all cases.

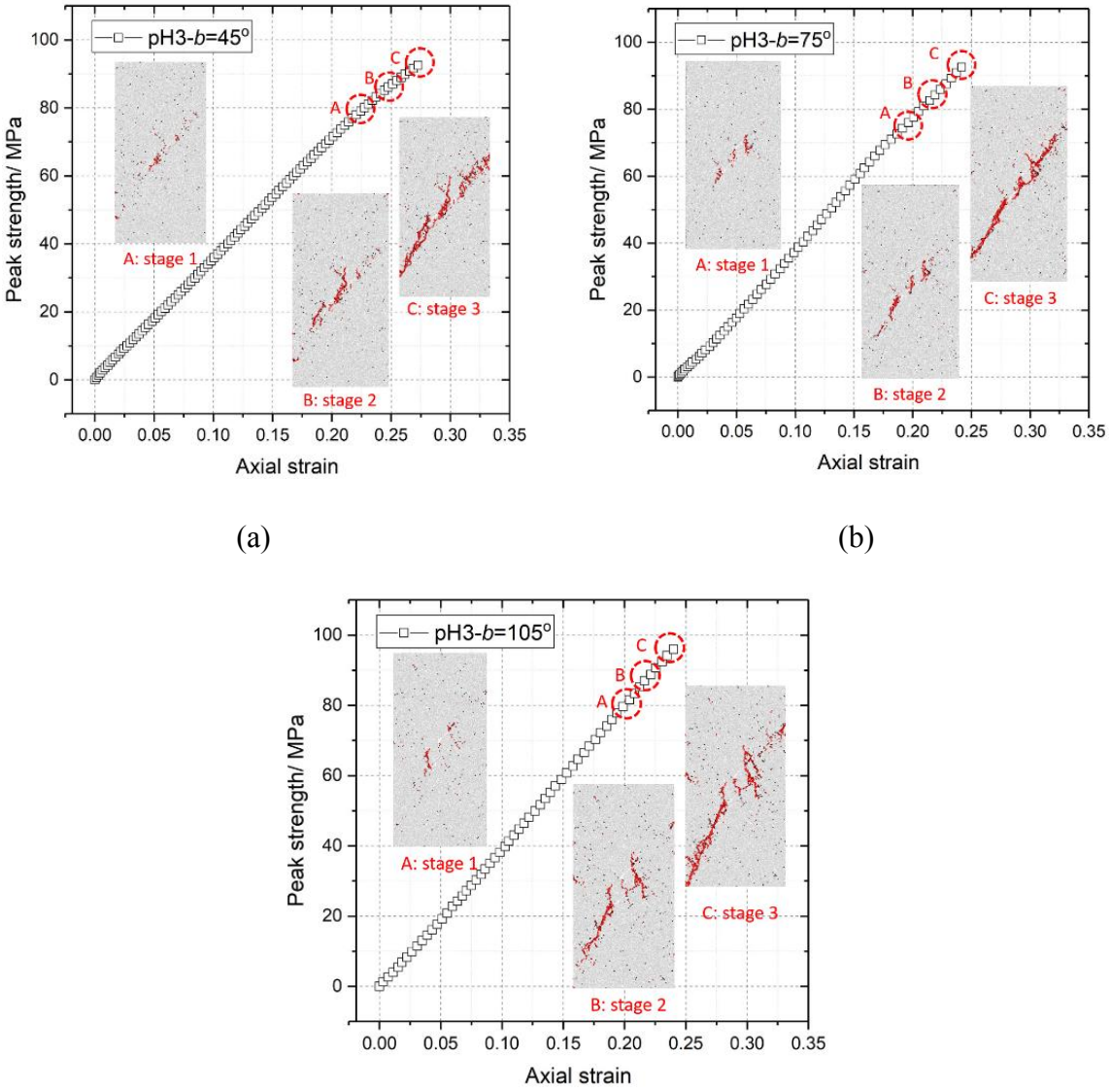

Fig.12 Crack development process of the BPM sample.
(Tensile cracks are red, and shear cracks in black.)

Under external loads, new cracks generate from the tips of pre-existing flaws and then propagate to the boundary of the sample. When the angle of inclination of the rock bridge is lower, such as β =45^o or β =75^o, the first wing cracks in the rock bridge between the two pre-existing flaws are connected to macro cracks in early compression stage; on the other hand, when the angle of rock bridge, β, is 105^o, micro cracks connect to macro cracks near the peak strength point.

5 Conclusions

Based on the micro damage law of the chemical corroded rock obtained by NMR and triaxial tests, a parallel-bonded chemical corrosion (PCC) model has been developed and applied in modelling rock fragmentations due to chemical corrosions. NMR is used to derive a micro damage accumulative model. Based on this micro damage accumulative model, the PCC model is developed and incorporated in a DEM simulation of corroded limestone. The formulation extends the functionality of the original bonded-particle model (BPM) by adding a chemically induced damage law to the bond.

An examination of chemical effects on crack initiation, propagation, coalescence and the mechanical properties of the limestone sample containing pre-existing flaws show that when the inclined angle of the rock bridge (β) is relatively low ,e.g., 45^o and 75^o, the wing cracks in the rock bridge region connects with bigger macro cracks as loading increases. Contrarily, when the inclined angle of the rock bridge (β) is 105^o, the development of wing cracks is isolated with no linkages to macro cracks. Chemical corrosion of rock decreases its peak strength and first crack initiation stress, which exacerbates crack generation.

Future work is planned to investigate the time-dependent chemical corrosion processes that occur in other types of rocks, such as granite or mudstone, and the deformation properties and stability of the rock under different stress conditions, such as creep or triaxial loads. To achieve this, further modifications of the micro damage cumulative model are required.

References

[1]SETO, M., NAG, D. K., VUTUKURI, V. S. & KATSUYAMA, K. Effect of chemical additives on the strength of sandstone[J]. International Journal of Rock Mechanics and Mining Sciences. 1997, 34(3):280.e1-280.e11.

[2]PATERSON, M. S. & WONG, T.-F. 2005. Experimental rock deformation-the brittle field, Springer Science & Business Media.

[3]ATKINSON, B. K. Stress corrosion and the rate-dependent tensile failure of a fine-grained quartz rock[J]. Tectonophysics. 1980, 65(3-4):281-290.

[4]HU, D., ZHOU, H., HU, Q., SHAO, J., FENG, X. & XIAO, H. A hydro-mechanical-chemical coupling model for geomaterial with both mechanical and chemical damages considered[J]. Acta Mechanica Solida Sinica. 2012, 25(4):361-376.

[5]FENG, X. T., CHEN, S. L. & ZHOU, H. Real-time computerized tomography (CT) experiments on sandstone damage evolution during triaxial compression with chemical corrosion[J]. International Journal of Rock Mechanics and Mining Sciences. 2004, 41(2):181-192.

[6]LI, S., ZHOU, Z., LI, X., LIU, L., HE, J. & LIU, Y. One CT imaging method of fracture intervention in rock hydraulic fracturing test[J]. Journal of Petroleum Science and Engineering. 2017, 156:582-588.

[7]GRIFFITH, A. A. & ENG, M. VI. The phenomena of rupture and flow in solids[J]. Phil. Trans. R. Soc. Lond. A. 1921, 221(582-593):163-198.

[8]GOL'DSTEIN, R. & SALGANIK, R. Brittle fracture of solids with arbitrary cracks[J]. International journal of Fracture. 1974, 10(4):507-523.

[9]BIENIAWSKI, Z. T. & BIENIAWSKI, Z. 1989. Engineering rock mass classifications: a complete manual for engineers and geologists in mining, civil, and petroleum engineering, John Wiley & Sons.

[10]ALONSO, E., ZANDARÍN, M. & OLIVELLA, S. Joints in unsaturated rocks: thermo-hydro-mechanical formulation and constitutive behaviour[J]. Journal of Rock Mechanics and Geotechnical Engineering. 2013, 5(3):200-213.

[11]CHAI, Z.-Y., KANG, T.-H. & FENG, G.-R. Effect of aqueous solution chemistry on the swelling of clayey rock[J]. Applied Clay Science. 2014, 93:12-16.

[12]CROIZÉ, D., BJØRLYKKE, K., JAHREN, J. & RENARD, F. Experimental mechanical and chemical compaction of carbonate sand[J]. Journal of Geophysical Research: Solid Earth. 2010, 115(B11).

[13]DEHKHODA, S. & HOOD, M. The internal failure of rock samples subjected to pulsed water jet impacts[J]. International Journal of Rock Mechanics and Mining Sciences. 2014, 66:91-96.

[14]GRGIC, D. & GIRAUD, A. The influence of different fluids on the static fatigue of a porous rock: Poro-mechanical coupling versus chemical effects[J]. Mechanics of Materials. 2014, 71:34-51.

[15]LAFRANCE, N., AUVRAY, C., SOULEY, M. & LABIOUSE, V. Impact of weathering on macro-mechanical properties of chalk: Local pillar-scale study of two underground quarries in the Paris Basin[J]. Engineering Geology. 2016, 213:107-119.

[16]ROHMER, J., PLUYMAKERS, A. & RENARD, F. Mechano-chemical interactions in sedimentary rocks in the context of CO2 storage: Weak acid, weak effects?[J]. Earth-Science Reviews. 2016, 157:86-110.

[17]TRIPATHI, R., SRIVASTAVA, M., HLOCH, S., ADAMČÍK, P., CHATTOPADHYAYA, S. & DAS, A. K. Monitoring of Acoustic Emission During the Disintegration of Rock[J]. Procedia Engineering. 2016, 149:481-488.

[18]XU, J., LI, S., TANG, X., TAO, Y. & JIANG, Y. Influential factors of acoustic emission location experiment of rock under uniaxial compression[J]. Chinese Journal of Rock Mechanics and Engineering. 2008, 27(4):765-772.

[19]ZHANG, Y., SUN, Q., CAO, L. & GENG, J. Pore, mechanics and acoustic emission characteristics of limestone under the influence of temperature[J]. Applied Thermal Engineering. 2017, 123:1237-1244.

[20]KAWAKATA, H., CHO, A., KIYAMA, T., YANAGIDANI, T., KUSUNOSE, K. & SHIMADA, M. Three-dimensional observations of faulting process in Westerly granite under uniaxial and triaxial conditions by X-ray CT scan[J]. Tectonophysics. 1999, 313(3):293-305.

[21]SATO, A. & OBARA, Y. Analysis of Pore Structure and Water Permeation Property of a Shale Rock by Means of X-Ray CT[J]. Procedia Engineering. 2017, 191:666-673.

[22]RAYNAUD, S., VASSEUR, G. & SOLIVA, R. In vivo CT X-ray observations of porosity evolution during triaxial deformation of a calcarenite[J]. International Journal of Rock Mechanics and Mining Sciences. 2012, 56:161-170.

[23]WONG, L. N. Y. & EINSTEIN, H. H. Crack Coalescence in Molded Gypsum and Carrara Marble: Part 1. Macroscopic Observations and Interpretation[J]. Rock Mechanics and Rock Engineering. 2009, 42(3):475-511.

[24]READ, R. & MARTIN, C. 1996. Technical summary of AECL's Mine-by Experiment

phase I: Excavation response. Atomic Energy of Canada Ltd.

[25]ZHOU, X., ZHANG, Y. & HA, Q. Real-time computerized tomography (CT) experiments on limestone damage evolution during unloading[J]. Theoretical and Applied Fracture Mechanics. 2008, 50(1):49-56.

[26]SINGH, R. 2016. Acoustic Emission Testing. In: SINGH, R. (ed.) Applied Welding Engineering (Second Edition). Butterworth-Heinemann.

[27]LANDIS, E. N. & KEANE, D. T. X-ray microtomography[J]. Materials Characterization. 2010, 61(12):1305-1316.

[28]ABDELGHANI, F. B., AUBERTIN, M., SIMON, R. & THERRIEN, R. Numerical simulations of water flow and contaminants transport near mining wastes disposed in a fractured rock mass[J]. International Journal of Mining Science and Technology. 2015, 25(1):37-45.

[29]CASTRO-FILGUEIRA, U., ALEJANO, L., ARZÚA, J. & IVARS, D. M. Sensitivity Analysis of the Micro-Parameters Used in a PFC Analysis Towards the Mechanical Properties of Rocks[J]. Procedia Engineering. 2017, 191:488-495.

[30]DING, X. & ZHANG, L. Simulation of rock fracturing using particle flow modeling: phase i-model development and calibration. 45th US rock mechanics/geomechanics symposium, 2011. American Rock Mechanics Association.

[31]POTYONDY, D. & AUTIO, J. Bonded-particle simulations of the in-situ failure test at Olkiluoto. DC Rocks 2001, The 38th US Symposium on Rock Mechanics (USRMS), 2001. American Rock Mechanics Association.

[32]SCHOLTÈS, L. & DONZÉ, F.-V. A DEM model for soft and hard rocks: Role of grain interlocking on strength[J]. Journal of the Mechanics and Physics of Solids. 2013, 61(2):352-369.

[33]MOHTARAMI, E., BAGHBANAN, A., EFTEKHARI, M. & HASHEMOLHOSSEINI, H. Investigating of chemical effects on rock fracturing using extended finite element method[J]. Theoretical and Applied Fracture Mechanics. 2017, 89:110-126.

[34]BEN ABDELGHANI, F., AUBERTIN, M., SIMON, R. & THERRIEN, R. Numerical simulations of water flow and contaminants transport near mining wastes disposed in a fractured rock mass[J]. International Journal of Mining Science and Technology. 2015, 25(1):37-45.

[35]PARK, B. & MIN, K.-B. Bonded-particle discrete element modeling of mechanical behavior of transversely isotropic rock[J]. International Journal of Rock Mechanics and Mining Sciences. 2015, 76:243-255.

[36]ITASCA CONSULTING GROUP, I. P. D. D. Particle Flow Code in 2/3 Dimensions[J]. Minneapolis, MN: ICG;. 2002.

[37]OSKAR POTYONDY, D. 2014. The bonded-particle model as a tool for rock mechanics research and application: Current trends and future directions.

[38]ASADI, M. S., RASOULI, V. & BARLA, G. A Bonded Particle Model Simulation of Shear Strength and Asperity Degradation for Rough Rock Fractures[J]. Rock Mechanics and Rock Engineering. 2012, 45(5):649-675.

[39]ZHANG, C., TU, S. & BAI, Q. Evaluation of Pore Size and Distribution Impacts on Uniaxial Compressive Strength of Lithophysal Rock[J]. Arabian Journal for Science and Engineering. 2017.

[40]CAI, M., KAISER, P. K., MORIOKA, H., MINAMI, M., MAEJIMA, T., TASAKA, Y. & KUROSE, H. FLAC/PFC coupled numerical simulation of AE in large-scale underground excavations[J]. International Journal of Rock Mechanics and Mining Sciences. 2007, 44(4):550-564.

[41]CHEN, W., KONIETZKY, H. & ABBAS, S. M. Numerical simulation of time-independent and-dependent fracturing in sandstone[J]. Engineering Geology. 2015, 193:118-131.

[42]SCHÖPFER, M. P. J., ABE, S., CHILDS, C. & WALSH, J. J. The impact of porosity and crack density on the elasticity, strength and friction of cohesive granular materials: Insights from DEM modelling[J]. International Journal of Rock Mechanics and Mining Sciences. 2009, 46(2):250-261.

[43]HAO LI , D.-M. Y., ZU-LIANG ZHONGB, YONG SHENG , XIN-RONG LIU Micro-damage evolution and macro-mechanical property degradation of limestone after chemical erosion (unpublished)[J]. Rock mechanics and mining sciences. 2018.

[44]KACHANOV, L. M. Rupture time under creep conditions[J]. International journal of fracture. 1999, 97(1-4):11-18.

[45]HOLT, R., KJØLAAS, J., LARSEN, I., LI, L., PILLITTERI, A. G. & SØNSTEBØ, E. Comparison between controlled laboratory experiments and discrete particle simulations

of the mechanical behaviour of rock[J]. International Journal of Rock Mechanics and Mining Sciences. 2005, 42(7):985-995.

[46]STEEFEL, C. I. & VAN CAPPELLEN, P. A new kinetic approach to modeling water-rock interaction: The role of nucleation, precursors, and Ostwald ripening[J]. Geochimica et Cosmochimica Acta. 1990, 54(10):2657-2677.

[47]POTYONDY, D. O. & CUNDALL, P. A. A bonded-particle model for rock[J]. International Journal of Rock Mechanics and Mining Sciences. 2004, 41(8):1329-1364.

[48]ALLIX, O. & HILD, F. INTRODUCTION TO CONTINUUM DAMAGE MECHANICS[J]. Continuum Damage Mechanics of Materials and Structures. 2002:235.

[49]HOLT, R. M., KJØLAAS, J., LARSEN, I., LI, L., GOTUSSO PILLITTERI, A. & SØNSTEBØ, E. F. Comparison between controlled laboratory experiments and discrete particle simulations of the mechanical behaviour of rock[J]. International Journal of Rock Mechanics and Mining Sciences. 2005, 42(7):985-995.

[50]CHO, N., MARTIN, C. D. & SEGO, D. C. A clumped particle model for rock[J]. International Journal of Rock Mechanics and Mining Sciences. 2007, 44(7):997-1010.

[51]ANDERSON, O. L. & GREW, P. C. Stress corrosion theory of crack propagation with applications to geophysics[J]. Reviews of Geophysics. 1977, 15(1):77-104.

[52]LAJTAI, E. Brittle fracture in compression[J]. International Journal of Fracture. 1974, 10(4):525-536.